Photochemical & Photobiological Sciences

Conservation and Diversity in the Secondary Forward Photodynamics of Red/Green Cyanobacteriochromes

Journal:	*Photochemical & Photobiological Sciences*
Manuscript ID	PP-ART-07-2019-000295.R1
Article Type:	Paper
Date Submitted by the Author:	27-Aug-2019
Complete List of Authors:	Gottlieb, Sean; University of California, Davis, Chemistry Chang, Che-Wei ; University of California-Davis Medical Center, Center for Biophotonics Jenkins, Adam; University of California, Davis, Chemistry Hayer, Randeep; University of California, Davis, Chemistry Martin, Shelley; University of California Davis, Molecular and Cellular Biology Lagarias, John Clark; University of California - Davis, Molecular and Cellular Biology Larsen, Delmar; University of California, Davis, Chemistry

8/27/2019 4:11 AM

Conservation and Diversity in the Secondary Forward Photodynamics of Red/Green Cyanobacteriochromes

Adam J. Jenkins[1#], Sean M. Gottlieb[1#], Che-Wei Chang[1#], Randeep J. Hayer[1], Shelley S. Martin[2], J. Clark Lagarias[2], and Delmar S. Larsen[1]*

[1]Department of Chemistry
University of California, Davis
One Shields Ave, Davis, 95616

[2]Department of Molecular and Cell Biology
University of California, Davis
One Shields Ave, Davis, CA, 95616

Running title: Secondary Photodynamics of Red/Green Cyanobacteriochromes

† This work was supported by a grant from the Chemical Sciences, Geosciences, and Biosciences Division, Office of Basic Energy Sciences, Office of Science, United States Department of Energy (DOE DE-FG02-09ER16117) to both J.C.L. and D.S.L.

* Corresponding Author: Delmar S. Larsen, Department of Chemistry, University of California, Davis, Davis CA 95616. Telephone: (530) 754-9075; E-mail: dlarsen@ucdavis.edu

[#]These authors contributed equally to the manuscript.

8/27/2019 4:11 AM

ABSTRACT

Cyanobacteriochromes (CBCRs) are photosensitive proteins that are distantly related to the phytochrome family of photoreceptors and, like phytochromes, exhibit photoactivity initiated by the excited-state photoisomerization of a covalently bound bilin chromophore. The canonical red-green photoswitching sub-family is the most studied class of CBCRs studied to date. Recently, a comparative study of the ultrafast (100 fs – 10 ns) forward photodynamics of nine red-green photoswitching CBCR domains isolated from *Nostoc punctiforme* were reported (Biochemistry, 2015, 54 (4), 1028-42). We extend this study by characterizing the secondary (10 ns -1 ms) forward photodynamics of eight red/green photoswitching CBCRs from *N. punctiforme* with broadband time-resolved absorption spectroscopy. We demonstrate that the dynamics of these representative red-green CBCRs can be separated into two coexisting pathways involving a photoactive pathway that is successful in generating the terminal light-adapted $^{15E}P_g$ population and an unsuccessful pathway that stalls after generating a meta-stable Lumi-Of intermediate. The photoactive pathway evolves through a similar mechanism from excitation of the dark-adapted $^{15Z}P_r$ state to generate a far-red absorbing Lumi-R_f and then via a succession of blue-shifting photointermediates to ultimately generate the $^{15E}P_g$ state. This suggests a steady deviation from planarity of the bilin chromophore during the dynamics. While, the general mechanism for this evolution is conserved among these CBCBs, the timescales of these dynamics deviate significantly. Only half of the characterized CBCRs exhibit the unproductive pathways due to photoexcitation of dark-adapted $^{15Z}P_o$ sub-population that upon photoexcitation generates a meta-stable Lumi-O_f intermediate, which eventually decays back to the $^{15Z}P_o$ population. $^{15Z}P_o$ is ascribed the binding of the "lid-tryptophan" that fails to π stack to the D-ring of the bilin in the dark-adapted state; its presence can be identified via enhanced absorption of high-energy tail of the electronic absorption spectrum.

8/27/2019 4:11 AM

INTRODUCTION

Nature has optimized light sensitive proteins over many millennia to efficiently couple photon absorption into useful biological photoactivity and includes important processes such as photo-induced homeostasis and photosynthesis.[1-3] Although the mechanisms underlying photo-induced homeostasis activity differ greatly depending on the nature of the relevant photoreceptor protein that initiates the signaling cascade,[4] they typically involve small photoinduced structural change of an embedded chromophore (often isomerization, although other mechanisms like electron transfer and adduct formation also occur) within protein scaffolding to trigger a cascade of events that results in large scale structural rearrangements required to propagate signaling pathways.

Phytochromes, which are multidomain proteins that bind linear tetrapyrole (bilin) chromophores and exhibit red (650-700 nm) and far-red (720-750 nm) sensitivity.[4, 5] These photoreceptors were initially discovered in plants and are responsible for light-induced responses such as shade avoidance and de-etiolation,[6, 7] but were subsequently discovered in algae, bacteria, cyanobacteria, and fungi.[5, 8-10] These broadly distributed photoactive proteins utilize different bilin chromophores depending on the organisms. For example, bacterial phytochromes use biliverdin-IXα (BV), while plant and cyanobacterial phytochromes utilize the more reduced phytochromobilin (PΦB) and phycocyanobilin (PCB) chromophores, respectively.[11] Photoexcitation of the bilin chromophore in the P_r dark-stable state of phytochrome (with its D-ring in a *15Z* configuration) initiates a photoisomerization reaction that generates a spectrally red-shifted primary Lumi-R intermediate (with its D-ring presumably adopting a *15E* configuration); this is the first step in a series of intermediates that ultimately results in the formation of the terminal light-adapted P_{fr} photoproduct.

Cyanobacteriochromes (CBCRs) photoreceptors are distantly related to phytochromes in binding bilin chromophores, but differ in their domain structure, photoactivity, and photochemistry.[2, 12] A distinguishing feature of CBCRs is that isolated bilin-binding cGMP-specific phosphodiesterases, adenylyl cyclases and FhlA (GAF) domains exhibit reversible *in vitro* photoactivity; phytochromes require the flanking domains to exhibit similar activity.[12-18] The *in vivo* phenotypic roles of only very few CBCRs have been elucidated to date.[19] For example, the SyPixJ1 CBCR mediates positive phototaxis in *Synechocystis*[20] and NpCcaS in *Nostoc (N.) punctiforme* responds to changing ambient light conditions by modulating the expression of light harvesting antennae via a process known as complimentary chromatic adaptation (CCA).[21, 22] Furthermore, The hormogonia filaments of *N. punctiforme* were shown to require the NpF2161-2168 locus for the phototactic response.[23]

The canonical red/green family is the most extensively studied class of CBCRs with both primary[18, 24-27] (100 fs to 10 ns) and secondary[28-32] (10 ns to 10 ms) dynamics reported. However, many questions remain unanswered, especially finding the key to predicting the behavior within the family. Recently, Gottlieb et al. reported a wide-ranging study focusing on the diversity of primary forward reaction ($^{15Z}P_r \rightarrow {}^{15E}P_g$) photodynamics of nine red/green CBCR domains from *N. punctiforme* with ultrafast transient absorption spectroscopy.[18] These dynamics exhibit diverse kinetics and photocycle spectral dynamics, implicating the importance of protein structure in modulating the primary photoactivities of the conserved PCB chromophore. The photodynamics of canonical red/green CBCRs were assigned to three classes (I, II and III) based on observation of zero, one, or two photoproducts within an ~10 ns timescale.[18] The subsequent secondary (10 ns - 1 ms) dynamics track the evolution of these photoproduct(s) into the light-adapted state through to the formation of multiple transient intermediates (Scheme 1). The primary forward dynamics

consisted of $^{15Z}P_r$* excited state and the primary ^{15E}Lumi-R_f photointermediate and in some cases the next intermediate, while the secondary forward dynamics capture the evolution of ^{15E}Lumi-R_f and the subsequent population to $^{15E}P_g$.[24, 33] The reverse dynamics complete the photocycle and involve the photoexcitation of the light-adapted $^{15E}P_g$ population and the subsequent evolution to regenerate $^{15Z}P_r$.

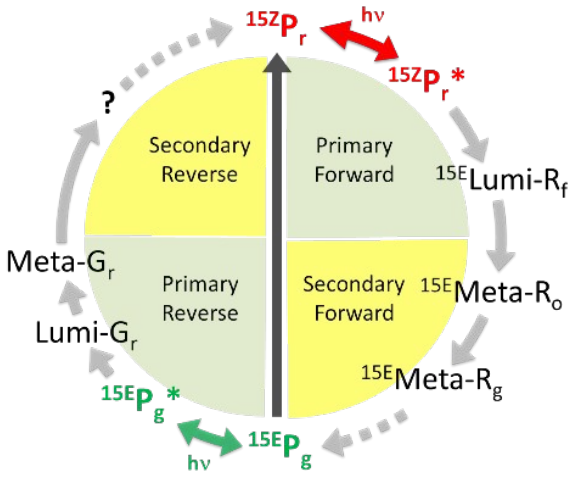

Scheme 1. Generalized red/green photocycle that comprised of the previously reported primary (150 fs – 8 ns) and secondary (550 ps – 1 ms) forward dynamics and primary reverse dynamics of NpR6012g4. The central black arrow going from $^{15E}P_g$ to $^{15Z}P_r$ represents dark reversion from the light state to the dark state.

The secondary dynamics for only a handful of CBCRs have been reported to date including NpF2164g3 [16] and NpF2164g7 [32] (B2J668), RcaE (Q47897),[34] NpR6012g4 (B2IU14),[33] AnPixJg2 (Q8YXY7),[29] NpR3784 (B2J457),[35] and Slr1393g3 (P73184).[36] The secondary forward dynamics of NpR6012g4 (red/green), NpF2164g7 (orange/green) and secondary reverse dynamics of RcaE (green/red) are unique among biliproteins since they exhibited heterogeneous dynamics beyond the primary dynamics timescale (>10 ns).[32, 34] The secondary forward dynamics of NpR6012g4 and secondary reverse dynamics of RcaE exhibited multiple spectrally heterogeneous Lumi photoproducts, where only one was photoactive in propagating to generate the light-adapted state.

The secondary dynamics of NpR6012g4 was published alongside wildtype and mutant NpR6012g4 NMR data that correlated this spectral inhomogeneity to heterogeneous ground state structures.[33] The secondary forward dynamics of Slr1393g3 (red/green) resulted in the isolation of two intermediates before forming $^{15E}P_g$ that differed from NpR6012g4 which exhibit a conserved mechanism of blue shifting intermediates, by having intermediates that are both blue shifted and red shifted of each other.[36]

These studies present a complex range of secondary dynamics in CBCRs including both homogeneous and inhomogeneous evolution, population merging (equilibration), shunting, and population collapsing. It is still unclear whether or not the secondary dynamics evolve through conserved mechanisms even for a specific sub-family. To address this, we collected the secondary dynamics (8 ns – 1 ms) using broadband transient absorption spectroscopy of eight red/green CBCR GAF domains isolated from *N. punctiforme*. This study complements the previous report of the primary dynamics (150 fs – 7.5 ns) of the same red-green CBCRs.[18]

MATERIALS AND METHODS

CBCR Purification and Characterization. The CBCRs GAF domains that were expressed were NpAF142g2, NpR1597g4, NpF2164g4, NpF2164g6, NpF2854g3, NpR4776g2, NpR4776g3, and NpR6012g4.[14, 18, 24, 25] The NpF2164g5 domain, explored in the Gottlieb et al. study,[18] was not characterized here since it is not a photoactive CBCR (i.e., does not generate a $^{15E}P_g$ state). Multiple sequence alignment of eight red/green GAF domains from *N. punctiforme* ATCC 29133 were performed using MUSCLE.[37] These sequences are aligned with the red/green CBCR domain AnPixJg2 (Q8YXY7), from *Anabaena* sp. PCC 7120 and the GAF domain of the phytochrome Cph1 (Q55168) from *Synechocystis* sp. PCC 6803 for comparison. A DNA region coding for each

8/27/2019 4:11 AM

GAF domain was amplified by PCR from *N. punctiforme* genomic DNA using appropriate primers, followed by cloning into the unique *Nco* I and *Sma* I sites of pBAD-Cph1-CBD.[38] Co-expression with PCB biosynthetic machinery in *E. coli* followed a published procedure,[39] and purification of GAF domains as intein-chitin binding domain (intein-CBD) fusions followed the procedure employed for *Synechocystis* Cph1.[38] After lysis, ultracentrifugation, and binding to chitin resin (NEB) in accordance with the manufacturer's instructions, intein cleavage was initiated by addition of DTT to the column, followed by overnight incubation at 4 °C. Peak fractions were pooled and dialyzed against TKKG buffer (25 mM TES-KOH pH 7.8, 100 mM KCl, 10% (v/v) glycerol) overnight prior to freezing in liquid nitrogen and storage at -80°C. Absorbance spectra were acquired at 25 °C on a Cary 50 spectrometer.

Transient Signals. The dispersed secondary transient absorption setup was constructed from two separate laser systems. The probe beam was derived from an amplified Ti:sapphire laser system (Spectra Physics Spitfire Pro + Tsunami) operating at 1 kHz, which produced 2.25-mJ pulses of 800-nm fundamental output with a 40-fs Full Width at Half Maximum (FWHM) duration.[40] This pulse train was used to generate the dispersed white-light continuum probe (440 – 750 nm) by focusing the laser pulses into a slowly-translating thick (10 mm) CaF_2 crystal.

Excitation pulses were generated by an independent diode-pumped solid-state Nd:YAG laser (Alphalas-A-532-300) with a fundamental 1064-nm output that was frequency-doubled to yield 532-nm pulses with a ~500-ps FWHM duration. The pump pulse train was set to 100 Hz electronically and locked to the ultrafast probe pulses with a pulse generator (Quantum Composers 9520) to produce difference spectra with respect to the non-pumped ground-state spectrum. The pump beam was electronically delayed with respect to the probe pulse, which allowed for ~10 ms

of temporal separation although only the <1 ms dynamics were free of artifacts from the excitation region flowing out of the probe region. Pump pulses were linearly polarized at 54.7^{o} (magic angle) with respect to probe pulses. The pump and probe pulse spot diameters at the sample were estimated at 200 μm and 50 μm, respectively, using a moveable razor blade. The greater pump pulse area minimizes artifact contributions to the signals due to varying spatial overlap between pump and probe beams, which was confirmed by monitoring changes in signal amplitude and spectral shape while dithering the pump beam with respect to the probe beam.

The temporal resolution of the experiment was estimated at ~550 ps using the rise time of transient signals. Samples were continuously flowed in a closed circuit to ensure fresh sample for each excitation pulse (though more slowly than for ultrafast experiments to ensure the measurement of long-time intermediates) and were continuously illuminated prior to entering the cuvette with ~5-mW of green (532 nm) laser diode to maintain the CBCR in the $^{15Z}P_r$ state during the experiment. The path length of the quartz cuvette was 2 mm and the samples were prepared with optical densities of 3-4 OD/cm (at the $^{15Z}P_r$ peak absorption wavelength). All experiments were performed at room temperature (25 °C).

To explore the role of excitation wavelength on the observed dynamics, the 1 ms spectra from the secondary data (with 532 nm excitation pulses) were compared to the 1 ms transient spectra collected from ultrafast signals (with ~640 nm excitation pulses),[18] which were collected by shifting the probe pulse slightly before (~1 ps) the pump pulse. To facilitate this, the sample flow rate is typically slowed down so that incomplete refreshing of new sample within the excitation laser volume in the flow cell. Under normal flow conditions, this pre-time zero signal (1 ms spectrum) is negligible. Subsequent “harmonic” dynamics (e.g., 4 ms) are not a major factor

in these spectra, since the flow rate has completely refreshed (within the excitation volume) on this timescale.

While the 532-nm excitation pulses used to initiate the secondary dynamics in this study are off resonant with the $^{15Z}P_r$ absorption spectrum of the CBCRs in the study (Figure 1E and S1; red curves), they are strongly resonant with the $^{15E}P_g$ spectrum (Figure 1E and S1; green curves). Consequently, the measured raw signals consist of both forward ($^{15Z}P_r \rightarrow {}^{15E}P_g$) and reverse ($^{15E}P_g \rightarrow {}^{15Z}P_r$) reaction signals. To extract the uncontaminated forward reaction signals, "clean" reverse reaction signals were first collected under continuous 630-laser diode illumination and 532 nm excitation (presented elsewhere) and were then subtracted from the mixed forward reaction signals to extract “true” forward reaction signals confirmed via the absence of bleach or photoproduct signals corresponding to the reverse dynamics. The raw signals can be found in Figure S2. For the rest of this paper, all references to transient signals are to the adjusted $^{15Z}P_r$ data.

RESULTS

The secondary forward photodynamics were collected and analyzed for eight red/green CBCR domains from *N. punctiforme*: NpAF142g2, NpR1597g4, NpF2164g4, NpF2164g6, NpF2854g3, NpR4776g2, NpR4776g3, and NpR6012g4.[14, 18, 24, 25] Of these eight GAF domains, the dynamics of two representative CBCR domains (NpF2164g6 and NpAF142g2) are emphasized to exemplify the longtime forward reaction dynamics. The NMR structures of the dark ($^{15Z}P_r$) and light ($^{15Z}P_g$) states [33] of NpR6012g4 are contrasted in Figure 1A-D with corresponding ground-state absorption spectra for NpR6012g4, NpF2164g4, and NpAF142g2 contrasted in Figure 1E. The spectral shapes of the $^{15Z}P_r$ absorption bands (red curves) of all CBCRs are qualitatively similar with a shoulder near 600 nm (Figure 1E and S1).[41] In contrast, the light-adapted $^{15E}P_g$

spectra (Figure 1E and S1; green curves) of almost all CBCRs are near Gaussian except for NpR1597g4 and NpR4776g2, where residual $^{15Z}P_r$ absorbance were still observed (Figure 1E and S1; red curves). The nomenclature previously outlined will used here where the parental states are abbreviated to $^{15C}P_{x,}$ where "C" represents the E/Z conformation of the chromophore and "x" is the spectral region of maximal absorbance. The photointermediates are represented by Lumi-X_a (initial photointermediate) or Meta-X_a (all secondary intermediates) where "X" was the spectral region of maximal absorption for the parental state that was excited and "a" is the spectral region of maximal absorption of the intermediate.[16] The secondary reverse dynamics are analyzed and discussed in detail elsewhere (manuscript in preparation).

The transient absorption (TA) spectra for all CBCRs domains at select delay times are contrasted in Figure 2. In general, TA spectra can be decomposed into a superposition of four overlapping signals:

(1) negative ground state bleach signal from the loss of ground-state absorption (GSB);

(2) negative stimulated emission (SE) signal attributed to excited-state $^{15Z}P_r^*$ populations;

(3) positive excited-state absorptions (ESA) from $S_1 \rightarrow S_n$ transitions induced from excited-state $^{15Z}P_r^*$ populations; and

(4) positive photoproduct absorptions (e.g., Lumi-$R_{f,}$) ascribed to photogenerated ground-state intermediate(s).

Although well resolved in the Gottlieb et al. study,[18] the excited-state signals (SE and ESA) are poorly resolved in the secondary data presented here, since the 550 ps instrument response (IRF) of the instrument poorly resolves these faster excited-state dynamics.

8/27/2019 4:11 AM

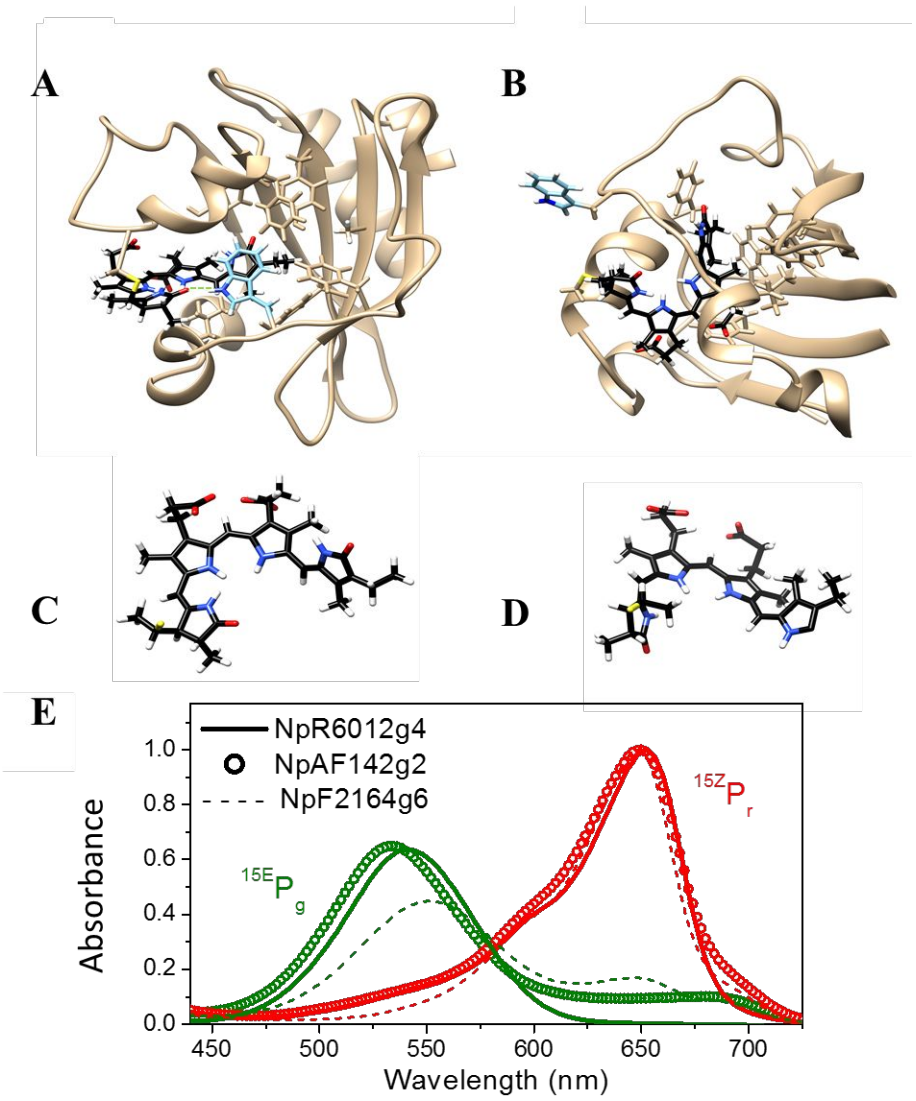

Figure 1. (A, B) NpR6012g4 protein structure around the dark (A; PDB 6BHN) and light (B; PDB 6BHO) states. Rings A through D of the bilin chromophore progress from left to right in alphabetical order. The dark state has hydrogen bonding between the Trp655 and A-ring of the bilin chromophore (dashed green line) as well as the Trp655 indole and bilin chromophore D-ring overlap (overlapped blue indole ring and black D-ring) resulting in π-stacking.[33] The chromophore of the light and dark states (C, D). Displacement of Trp655 away from the chromophore due to the isomerization event, causing the loss of the interactions between the chromophore and Trp655. (E) The static ground state absorbance of the dark (red) and light (green) states for NpR6012g4 (solid lines), NpFA142g2 (open circles), and NpF2164g6 (crossed curves).

The spectral evolution of the TA signals for nearly all the CBCRs follows similar pathways with monotonically blue-shifting intermediates from primary Lumi-R_f (peaking around 675 nm) generated by the decay of the excited-state $^{15Z}P_r$ * populations to generate $^{15E}P_g$ (peaking betwen 550-575 nm). These primary intermediates absorb in the yellow and orange regions of the spectrum (Figure 2A and 2C). The amplitude of the negative GSB increases as the Lumi-R_f population with an overlapping positive absorption shifts to the subsequent Meta intermediates (Scheme 1). On slower timescales, the absorption bands ascribed to the subsequent orange absorbing Meta-R_o and yellow absorbing Meta-R_y intermediates blue-shift to yield green-absorbing bands ascribed to Meta-R_g that in many of the CBCRs closely resembles $^{15E}P_g$ (Figure 1E) indicating the photoreactions are mostly completed on a <10 ms timescale (at least with respect to the bilin electronic absorption spectrum). The >1-ms TA difference spectra for all CBCR, where the excited sample progress to flow out of the excitation region, are compared in the Supporting Information (Figure S3).

8/27/2019 4:11 AM

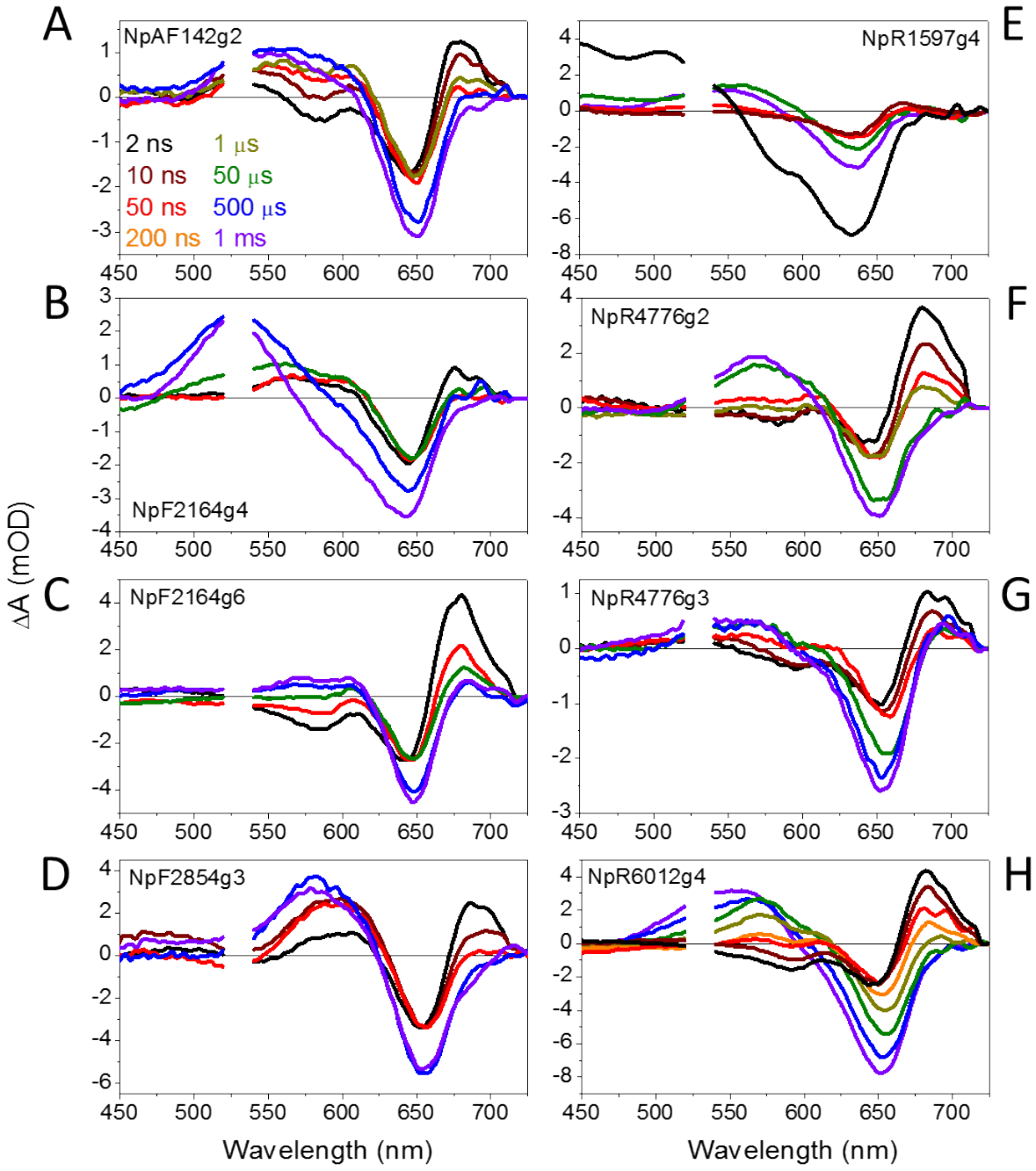

Figure 2. Transient absorption difference spectra for: (A) NpAF142g2, (B) NpF2164g4, (C) NpF2164g6, (D) NpF2854g3, (E) NpR1597g4, F) NpR4776g2, (G) NpR4776g3, and (H) NpR6012g4. Spectra colors correspond to the probe times specified in the legend in panel A. Not all probe times are represented for each CBCR. A narrow spectral window around the 532 nm excitation wavelength was excised due to pump scattering.

While the transient absorption (TA) of the CBCRs share similar spectral features, the kinetic traces in Figure 3 show key differences in the timescales. The traces clearly show the shared dynamic trends between the CBCRs: ^{15E}Lumi-R_f photoproduct (680 nm, black curve), $^{15Z}P_r$ ground state bleach band (650 nm, red curve), and subsequent blue-shifted ^{15E}Meta-R_o, ^{15E}Meta -R_y, and ^{15E}Meta -R_g photoproducts (590 nm, orange and 550 nm, green curves). For NpF2164g6, the primary Lumi-R_f intermediate (black trace) decays within 1 μs to generate the secondary Meta-R_y intermediate (orange and green traces). NpAF142g2,NpF2164g6, and NpR4776g3 follow a similar progression, but with a primary Lumi-R_f photoproduct (black trace) that persists for 50 μs and 500 μs, respectively (Figure 3A,3C, and 3G). Dissimilarities such as these are observed in the other CBCRs as well (Figure 3).

NpF2854g3 (Figure 3D) also exhibits dynamics starkly different from those of the other CBCRs. Gottlieb et al. reported that NpF2854g3 generates Meta-R_o more quickly than the other CBCRs,[18] and a similar progression is observed in these secondary dynamics, as NpF2854g3 evolves into a positive band at 590 nm (orange data and curve) more quickly than any of the other CBCRs. The amplitude of the 590-nm trace for NpF2854g3 is reflected in the kinetic trace of the GSB (650 nm, red data and curve), suggesting the absorption band near 590 nm shifts back and forth, overlapping with the bleach band to different extents over time. This suggests that NpF2854g3 exhibits more complex structural rearrangements on this particular timescale than the other CBCRs, such as an equilibrium between a Meta-R_o and a Meta-R_y photointermediates that later coevolve to a Meta-R_g. In addition to the more complex photodynamics exhibited of NpF2854g3 compared to the other CBCRs presented here, NpF2854g3 exhibited a weakening of the signal at all wavelengths on the same timescale (90μs – 1 ms; Figure 3D), suggesting that there is a shunt from the Meta-R_g photointermediate back to the $^{15Z}P_r$ ground state. NpF1597g4 had

8/27/2019 4:11 AM

weaker absorbance in the far-red region and fast filling in of the bleach due to low Lumi-R_f quantum yields as previously reported.[18]

In Figure 4, transient absorption difference spectra from the previous ultrafast study[18] are compared with those from the present study for the two representative CBCRs at probe times specified in the panels (2 ns, 7 ns, and 1 ms after excitation). The data are qualitatively similar, although with some important differences in the 550-620-nm region for both CBCRs, where the amplitudes of the 532 nm excitation signals are generally more negative than that of the red-excitation data. This indicates a loss of an absorbing population in that region for the green-excitation data, or a GSB near 600 nm (orange spectral region) belonging to a separate population not present after red excitation. Here the 1 ms data for both datasets for each CBCR exhibit similar spectra (Figure 4C, and F). These trends were also observed in the 2 ns and 1 ms spectra after 532 nm and 650 nm excitation of NpR6012g4. This may possibly be arising from a distinct ground-state subpopulation coexisting with $^{15Z}P_r$ being preferentially excited by the 532-nm pulses, namely $^{15Z}P_o$ which was previously reported Lim et al. for NpR6012g4.[33]

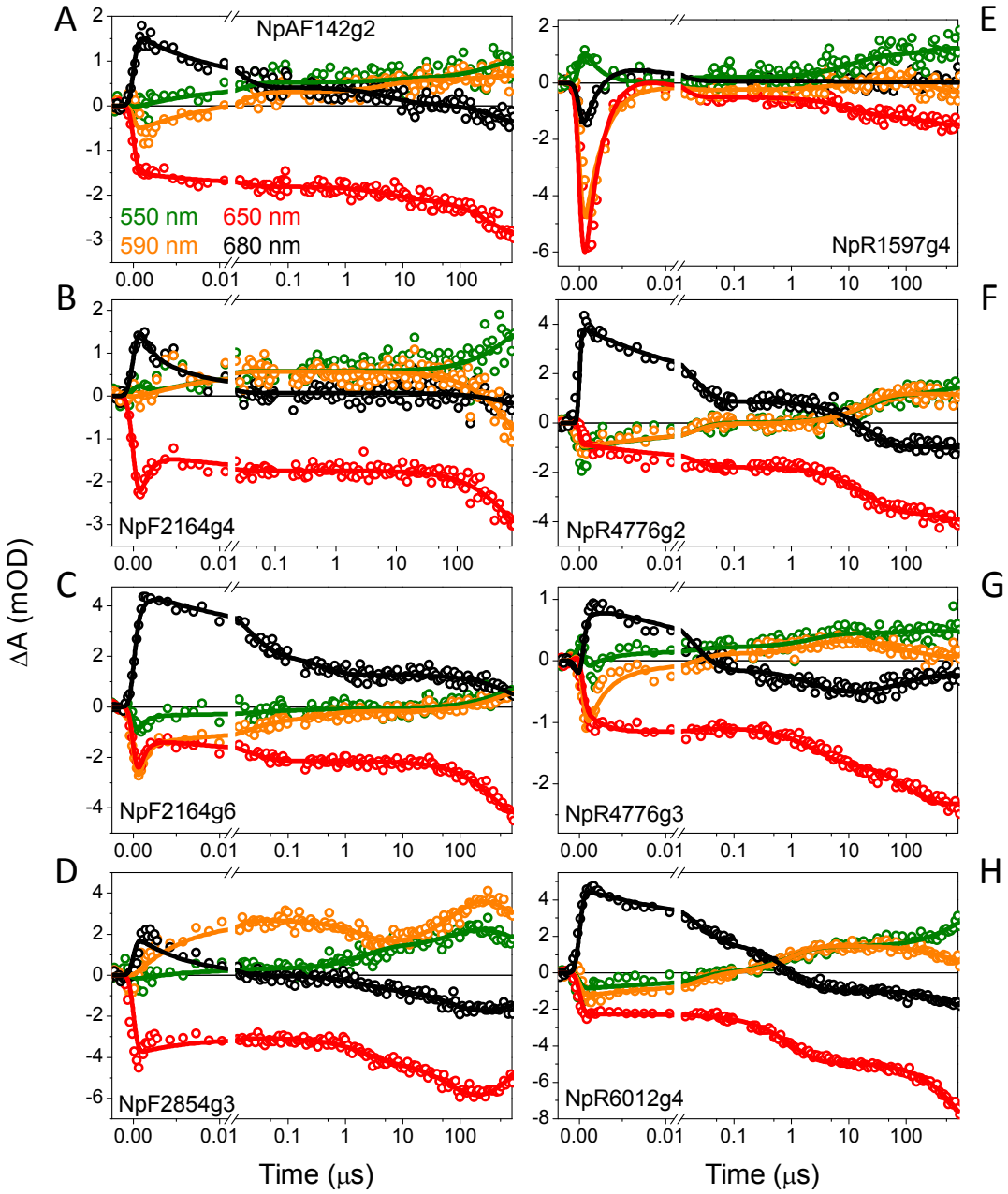

Figure 3. Kinetic traces for: (A) NpAF142g2, (B) NpF2164g4, (C) NpF2164g6, (D) NpF2854g3, (E) NpR1597g4, F) NpR4776g2, (G) NpR4776g3, and (H) NpR6012g4. Spectra colors correspond to the wavelengths specified in the legend in panel A. Data (open circles) are overlaid with fits (solid curves) extracted from the target model for each respective CBCR (Figure 5 and Table 1).

8/27/2019 4:11 AM

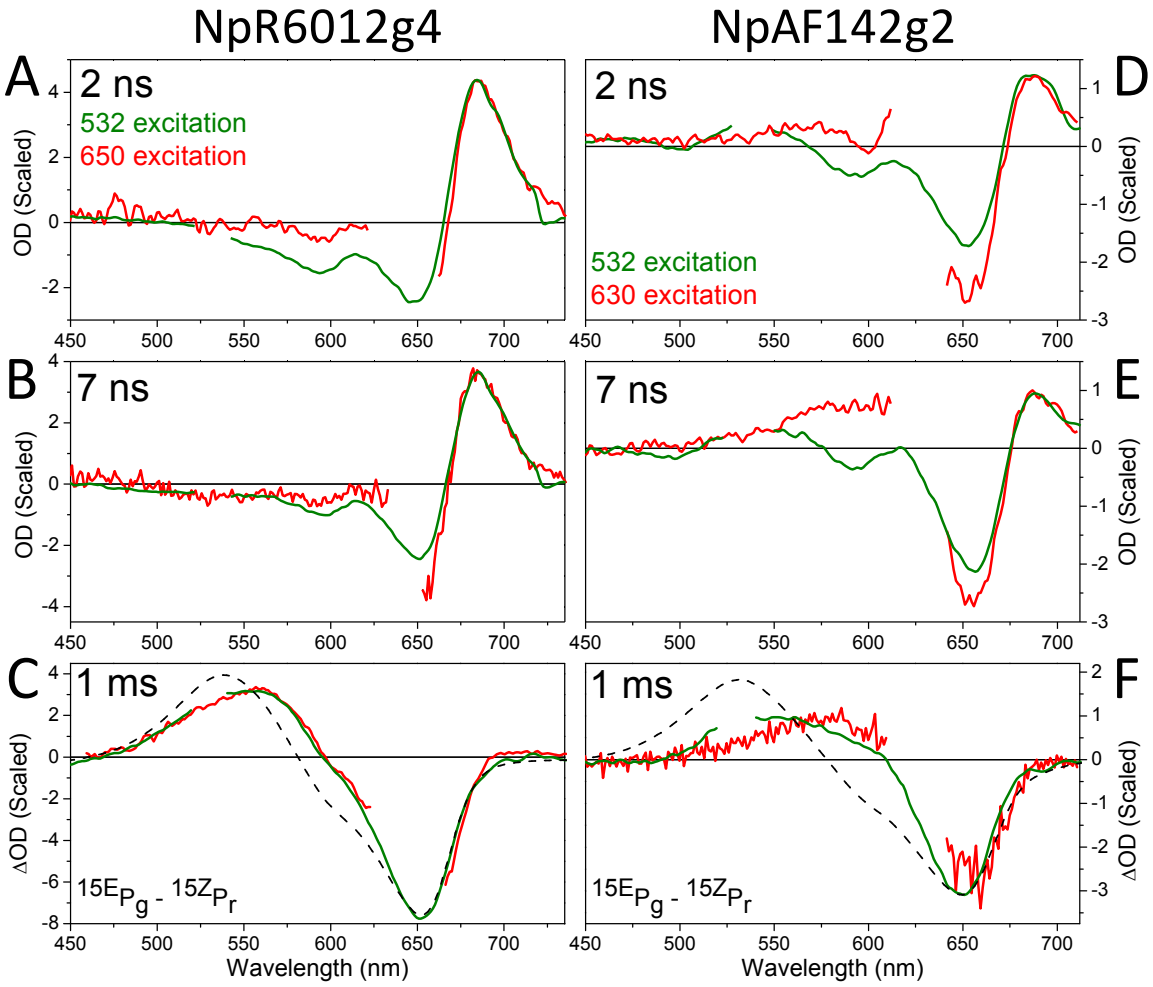

Figure 4. Comparison of transient absorption difference spectra for NpR6012g4 and NpAF142g2 after 630-nm or 650-nm excitation (red curves) discussed in detail in primary forward photodynamics of red/green CBCRs survey with after 532-nm excitation (green curves) at 2 ns (A and D), 7 ns (B and E), and 1 ms (C and F).[18] For NpF2164g6 (A, B, and C), note the relative differences in amplitude near 600 nm in the bleach band in A and B. NpAF142g2 (D, E, and F) exhibits amplitude and signal differences in the bleach band and in the 550-600-nm region of the secondary photoproduct. Ground-state $^{15E}P_g$ - $^{15Z}P_r$ difference spectra are overlaid with the 1 ms spectra (C and F, grey dashed curves).

GLOBAL ANALYSIS

Sequential models (state 1 → state 2 → state 3 → state 4, etc.) were initially used to fit the TA data (Figure 5 and S4 and Table 1) resulting in evolution associated difference spectra (EADS) of increasing lifetimes for each population in the sample. This approach is useful in identifying the underlying **"**apparent**"** (i.e., experimentally observed) timescales in the data, but does not necessarily decompose the apparent timescales into the microscopic timescales of co-evolving populations.[42, 43] This requires a more complex non-sequential target analysis to adequately address *a priori* knowledge to the system of interest.[13, 24] However, the sequential EADS analysis can be used to extract useful timescale information in the systems.[14, 24] In addition to the sequential model, a parallel model using the same time constants as the sequential model, and the result difference associated difference spectra (DADS) can be found in the supplemental information (Figure S6).

All TA signals were fit to sequential models consisting of up to five compartments (Figures S6 and S7). For several of the CBCRs, including the representative CBCRs, certain features of the forward reaction EADS indicate complex underlying dynamics after excitation involving multiple photoproduct populations that progress with strong spectral and temporal overlap. For example, in the case of NpR6012g4, EADS1 and EADS2 share a similar absorption band in the 670-720-nm region, albeit with differing amplitudes (Figure S5D). On the same timescale, the 550-620-nm negative region in EADS1 decays to near zero in EADS2. This evolution indicates at least two separate populations are represented by EADS1 that decay on different timescales. The decay of the shorter lived state from P_o accounts for the decay of the negative signal between EADS1 and EADS2. This inhomogeneity was also readily apparent when comparing the 532 nm and 650 nm excitation spectra as selected times (Figure 4), which showed that the higher energy excitation

8/27/2019 4:11 AM

resulted in a stronger positive absorption signal from 550 – 620 nm since the $^{15Z}P_o$ state is preferentially excited with the 532 nm excitation pulse, but not the 650 nm. The existence of another longer living population originating from P_r justifies the relative persistence of the positive absorption band near 680 nm in EADS2. Furthermore, while the positive band near 680 nm decays to ~50% of its original amplitude between EADS1 and EADS2, the same trend is not observed for the bleach band near 650 nm further indicating underlying heterogeneous dynamics. Similar trends are observed in the EADS for NpAF142g2 (Figure S5A), NpF2164g6 (Figure S5B), and NpR4776g2 (Figure S5C).

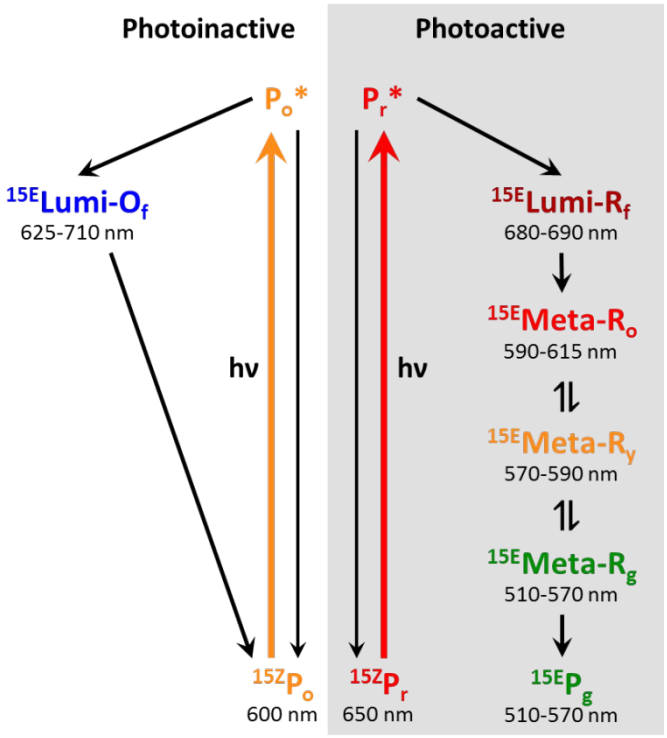

Figure 5. General photocycle model and proposed reaction pathway for the forward reaction of the CBCRs in the present study at 532-nm excitation. $^{15Z}P_o$ and $^{15Z}P_r$ are initially activated by light to generate the primary ^{15E}Lumi-O_f and ^{15E}Lumi-R_f intermediates. $^{15Z}P_r$ generates ^{15E}Lumi-R_f, propagates the photocycle to eventually generate $^{15E}P_g$, while ^{15E}Lumi-O_f decays back into the original $^{15Z}P_o$ state. Labels for intermediates are color-coded to the EADS in Figure 6.

A generalized target model was constructed to fit the TA data of each CBCR (Figure 5) with corresponding EADS (Figure 6) and concentration profiles (Figure S7). Timescales for all CBCRs are listed in Table 1. Timescales and EADS for excited-state species ($^{15Z}P_r$* and $^{15Z}P_o$*) are omitted from Table 1 and Figure 6, where applicable (see the Gottlieb at al.[18] for more details).

Table 1. Timescales extracted from the sequential EADS analysis for the CBCRs in this study. The corresponding EADS are shown in Figure 6. *Species exhibited unproductive Lumi-O_f pathway. The percent of the population that evolves through these pathways are presented in the two far right columns. **The final timescale contains phase attributed to the flow of the irradiated sample volume out of the probe volume.

Sample	Lumi-Of	EADS0	EADS1	EADS2	EADS3	% L-Of	%EADS
NpAF142g2*	7 µs	11 ns	865 µs	>3 ms**	-	21	79
NpF2164g4	NA	8 ns	825 µs	>3 ms**	-	0	100
NpF2164g6*	45 ns	555 µs	>3 ms**	-	-	67	33
NpF2854g3	NA	6 ns	2.2 µs	80 µs	2.8 ms**	0	100
NpR1597g4	NA	5.5 ns	8.5 µs	220 µs	>3 ms**	0	100
NpR4776g2*	16 ns	21 µs	510 µs	>3 ms**	-	77	23
NpR4776g3	NA	190 ns	2.5 µs	110 µs	>3 ms**	0	100
NpR6012g4*	21 ns	1 µs	880 µs	>3 ms**	-	60	40

Not all CBCRs exhibit inhomogeneous dynamics, as several CBCRs show no apparent Lumi-O_f photoproduct stemming from $^{15Z}P_o$. These CBCRs required only sequential EADS analyses to yield appropriate models and corresponding species associated difference spectrum (SADS) for microscopic populations, only utilizing the shaded region of the target model (Figure 5). The effectiveness of these models for describing the data is demonstrated via the excellent agreement between the simulated kinetics traces and raw data in Figure 3. This target model differed significantly from the one used to fit the secondary forward dynamics for NpF2164g7 (orange/green), which proposed a more complex heterogeneous model.[32]

8/27/2019 4:11 AM

The various spectral regions of the EADS or SADS of the eight CBCR domains compared in Figure 6, are highlighted with their respective color to help visualize the Lumi-O_r, Lumi-R_f, Meta-R_o, Meta-R_y, and Meta-R_g spectra that compose the EADS and the trend of the evolution.

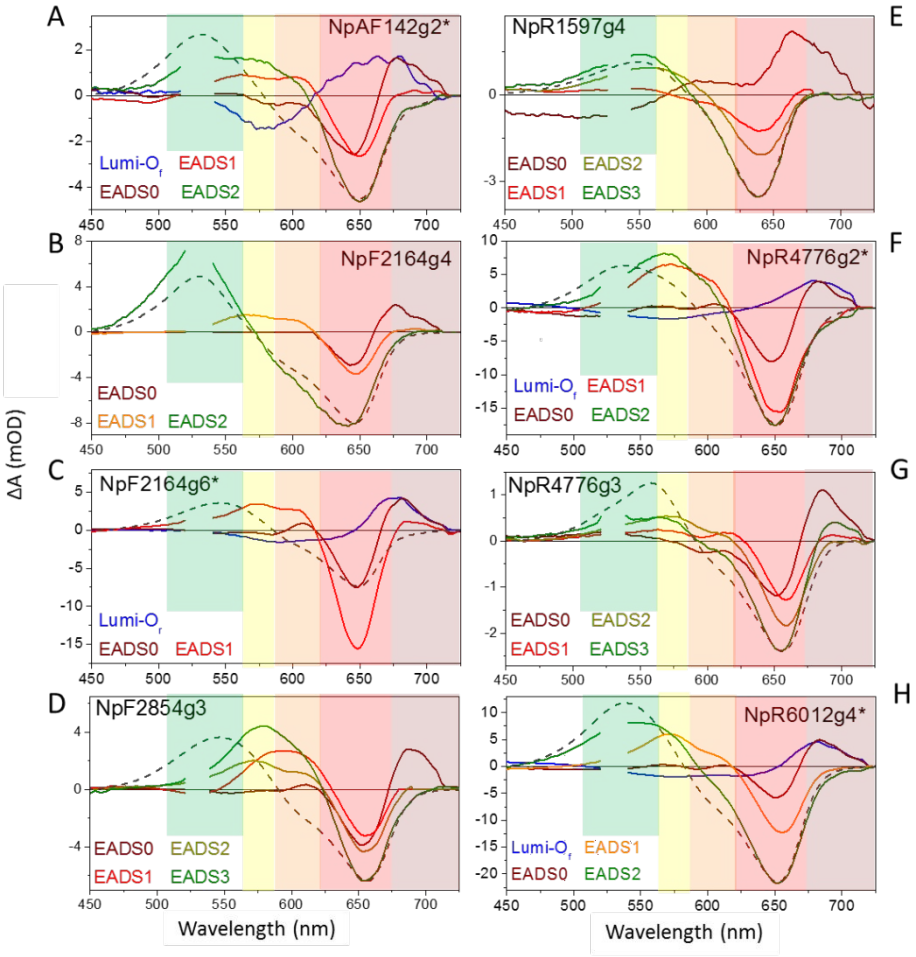

Figure 6. Evolution associated difference spectra (EADS) for the eight CBCRs as extracted from the model in Figure 5 and kinetic parameters in Table 1. The $^{15E}P_g$ – $^{15Z}P_r$ difference spectra scaled to coincide with other signals are plotted for comparison (dashed curves). The Lumi-R_f population for NpR1597g4 (E, dark red curve) was poorly resolved due to its low yield and rapid lifetime. Excited-state SADS are not shown, if resolved. The different spectral regions of the EADS are highlighted to assist is the visualizing the various intermediates where far-red is represented by wine and all the other visible wavelength regions are represented with their respective colors. Each sample that exhibited evidence of the photoinactive $^{15Z}P_o$ subpopulation are indicated with an asterisk in the panel label.

All eight studied CBCRs presented here followed a simple evolutionary mechanism within the ~1 ms probe window. Even though NpF2164g7 had a more complex heterogeneous model, the blue-shifting of the subsequent intermediates was also observed.[32] The secondary forward dynamics of NpF2164g6 ($^{15Z}P_r \rightarrow {}^{15E}P_g$) exhibit similar trends of the reverse reaction of RcaE ($^{15E}P_r \rightarrow {}^{15Z}P_g$), where there was a long lived Lumi state that evolved to a Meta state. NpF2164g6 had a Lumi decay constant of 556 μs, compared to the 110 μs decay constant of the RacE Lumi-R_f state, making is the longest lived primary photoproduct to resolved to date (Table 1).[29, 34, 36] NpR1597g4 exhibits an exceptionally longer-lived excited state (Figure 3E) than the other CBCRs, as evidenced by the traces up to 3-4 ns and the lack of a clear Lumi-R_f photoproduct absorption near 680 nm (Figure 2E), also characterized in ultrafast signals.[17, 18] While NpR1597g4 does exhibit slight positive signals at 680 nm, the Lumi-R_f spectrum extracted from the target model does not agree with those of the other CBCRs (Figure 6).[18] The Lumi-R_f spectrum for NpR1597g4 shows negative signals in the blue and green regions, where the other CBCRs' Lumi-R_f populations are near-zero. This discrepancy is likely due to the extraction of a low-yielding Lumi-R_f photoproduct spectrum from the signals and not an accurate representation of the Lumi-R_f spectrum.

Uniquely, NpR4776g3 deviated from this conserved mechanism of blue shifting intermediate observed in the 7 other CBCRs domains by exhibiting a far-red absorbing state that was populated after Meta-R_g (Figure 6G; yellow and green curves). It is unclear what is causing this red-shifted state and is a matter of further investigation.

DISCUSSION

The secondary (>10 ns) forward ($^{15Z}P_r \rightarrow {}^{15E}P_g$) broadband TA signals of eight red/green photoswitching CBCR GAF domains display the diversity in their secondary dynamics. While all

8/27/2019 4:11 AM

CBCRs studied share similar ground-state absorption spectra (Figure 1 and S1), the previously reported primary (<10 ns) signals exhibited stark differences in photoproduct quantum yields and excited-state and photoproduct dynamics and reveled that there are at least three different classes: Class I characterized by no, or little Lumi formation, class II characterized by Lumi formation, but no apparent evolution to a Meta state on an ultrafast timescale (< 8 ns), and class III which did have Meta formation on the ultrafast timescale.[18] While these CBCRs share certain similarities beyond the ultrafast timescale, key differences in timescales are observed in the secondary time regime (>10 ns).

Productive Photodynamics. Most of the CBCRs exhibit similar multiphase evolution from excitation of $^{15Z}P_r$ to generation of $^{15E}P_g$. From the kinetic traces in Figure 3, positive signals in the orange and green (590-520 nm) arise from Lumi-R_f decay and are attributed to Meta-R populations. This monotonic evolution can be attributed to similar protein scaffolds near the chromophore during the reaction.[29, 44] Previously, Velazquez and coworkers suggested the importance of the Trp residue stacked onto the D-ring of the chromophore of AnPixJg2 in moderating the isomerization of the chromophore after photoexcitation.[45] This Trp would be expected to be a major component for many CBCRs in progressing the chromophore through the photocycle from $^{15Z}P_r$ to $^{15E}P_g$, as this Trp is highly conserved in red/green photoswitching CBCRs.[44] Recently, Rockwell and coworkers argued against the importance of the conserved Trp through identification of two highly conserved phenylalanine (Phe) residues essential for evolution of the $^{15E}P_g$ ground-state.[44] These two Phe residues are conserved in six of the eight CBCRs in this paper. In the two outliers, NpR1597g4 incorporates methionine (Met) in the place of the helix Phe and NpR4776g3 incorporates tyrosine (Tyr) and isoleucine (Ile) in place of both the β2 and helix

Phe residues, respectively (Table S1). ^{15E}The replacement of the two Phe residues in NpR4776g3 may be the cause of the observed Meta-R_f state observed in NpR4776g3 where the chromophore becomes less structurally deformed due to a less rigid protein structure near the D-ring of the chromophore (Figure 1). This Meta-Rf state evolved by 2 ms since it is not apparent in the 1 to 3 ms (Figure S3G).

In contrast to the monotonic evolution from Lumi-R_f to $^{15E}P_g$ observed in most red/green CBCRs, NpF2854g3 is more complex, exhibiting biphasic growth (Figure 3D; yellow curve), despite its conservation of the two aforementioned Phe residues.[44] The amplitude of the 590-nm kinetic trace for NpF2854g3 first peaks near 50 ns after excitation, only to reach a relative minimum at ~7 μs. The signal then increases, reaching maximum amplitude near 250 μs and decaying past the 1 ms probe delay window. A similar non-monotonic trend is observed in the dynamics at the other wavelengths (Figure 3D), stemming from the overlap of multiple populations in those spectral regions. The kinetics for NpF2854g3 indicate the absorption maxima of secondary intermediates shift back and forth between 50 ns and the end of the probe delay window, not following the unidirectional evolution observed in the other CBCRs. The NpF2854g3 EADS in Figure 6D more clearly depict the shifting of the ground-state intermediate absorption bands. Like many of the CBCRs studied, NpF2854g3 generates a Lumi-R_f photoproduct that absorbs near 680 nm and decays into Meta-R_o near 600 nm. The Meta-R_o band, then, blue-shifts to yield Meta-R_y. Strikingly, the Meta-R_y absorption band peaking at 570 nm red-shifts to yield an absorption band of increased amplitude peaking near 580 nm. This new band, attributed to Meta-R_{y2}, does not undergo any clear shifting within the 1 ms probe delay window, although the amplitude of the signal does decrease. Dynamics comparable to those described for NpF2854g3 were not observed for any other red/green CBCR. The 680 nm kinetic trace for NpR4776g3 also showed weak signs

8/27/2019 4:11 AM

of a biphasic growth that was also apparent in the transient absorption spectra (Figure 3G) and Meta-R_g EADS (Figure 6G; green curve), but this was attributed to contamination from the reverse reaction ($^{15E}P_g \rightarrow {}^{15Z}P_r$) that was not successfully removed from the adjusted data since the reverse reaction has positive absorption in this region around this time after excitation (Figure S1)

Similar dynamics to NpF2854g3 were detected in the secondary dynamics for the violet/orange NpF2164g3 CBCR in the reverse direction.[16] For NpF2164g3, the initial Lumi-O_r photoproduct decays on a 9-ns timescale into Meta-O_g. The photocycle and spectral sensitivity of NpF2164g3 are greatly influenced by the presence of a second Cys linkage at carbon 10 of the PCB chromophore.[16, 46] However, instead of blue-shifting further to generate $^{15Z}P_v$, Meta-O_g decays on a 750-ns timescale to yield an orange-absorbing Meta-O_r intermediate peaking near 650 nm. Furthermore, the 1 ms spectrum collected for NpF2164g3 exhibits a positive absorption peaking near 630 nm. This indicates the reverse reaction of NpF2164g3 is slow to generate $^{15Z}P_v$ from $^{15E}P_o$, and that it progresses in a more complex pathway of intermediates, compared with many red/green CBCRs, including AnPixJg2.[16, 29] NpF2164g3 does not belong to the red/green photoswitching family and displays certain structural and spectroscopy discrepancies from these CBCRs, but arose within the red/green subfamily based upon evolutionary relationships.[46, 47] Moreover, NpF2164g3 also lacks the two Phe residues conserved in many of the red/green CBCRs.[16, 44] The effects of structural residue modification on the photoactivity of NpF2164g3 have yet to be discovered.[16] The similarities shared between the forward reactions and sequences of the CBCR domains studied and mentioned here may indicate parallel evolutionary origin and function for several of these CBCRs. However, this study alone cannot fully address this hypothesis.

Nonproductive Photodynamics. The dark adapted ground state spectra for all the domains studied here are compared in Figure 7A with a zoomed in spectra of the green region presented in Figure 7C that showed that all of the domains exhibit small, but non-zero absorption at 532 nm, making it possible to initiate forward reaction dynamics with 532-nm pump pulses.[18] Upon excitation with 532-nm pulses, NpAF142g2, NpF2164g6, NpR4776g2, and NpR6012g4 exhibited broader and slightly blue-shifted photoproduct absorption and a prominent 600-nm GSB (Figure 6). The four CBCRs that displayed Lumi-O_r photoproducts, with the exception of NpF2164g6, generally exhibit greater positive absorption in the more blue shifted wavelengths in the static spectra (Figure 7D).

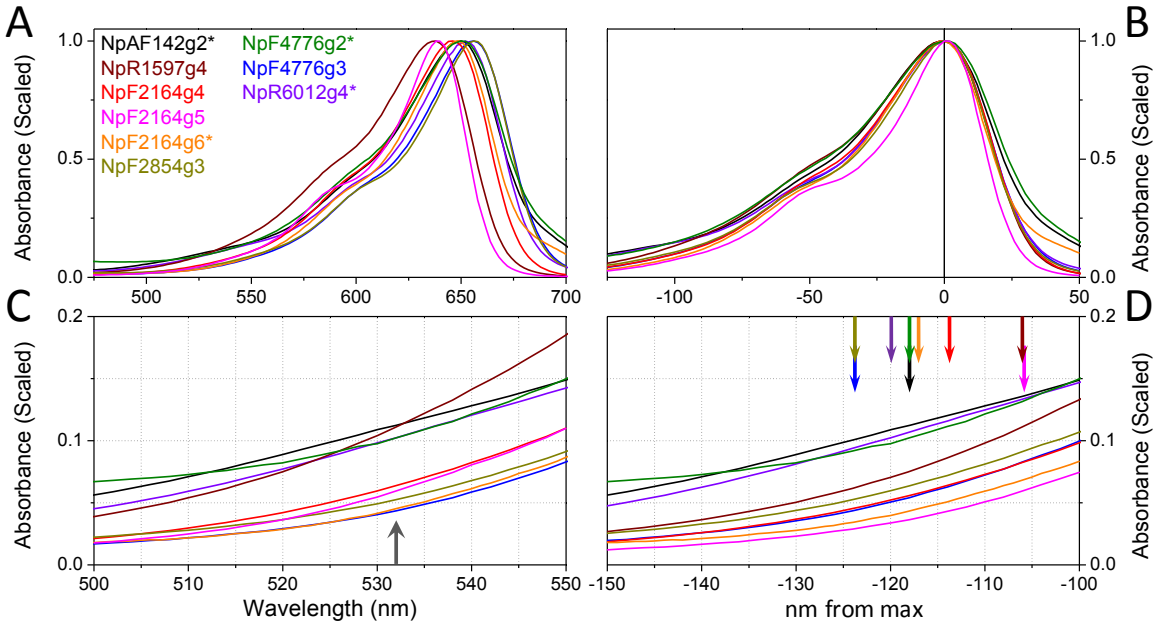

Figure 7. (A) $^{15Z}P_r$ ground-state absorption spectra for all CBCRs in this study, normalized at the wavelengths of maximum absorbance. The samples that exhibited the unproductive $^{15Z}P_o$ state is indicated with an asterisk. (B) Absorption spectra from panel A, shifted to coalesce the wavelengths of maximum absorbance. (C) Spectra from panel A, focusing on the spectral region near the excitation wavelength (532 nm, grey arrow). (D) Shifted absorption spectra from panel B, focusing on the spectral region near the excitation wavelength (532 nm, represented by arrows color coded to match the legend in panel A).

8/27/2019 4:11 AM

The generalized target model for the red/green CBCRs is presented in Figure 5, which has been previously reported for NpR6012g4,[33] has the presence of photoinactive Lumi-O_f and photoactive Lumi-R_f subpopulations that arise due to an out or in orientation of Trp655 and horizontal or vertical orientations of the Asp657 residue (Figure 8), respectively. Ten percent of reported structures of NpR6012g4 incorporated an "out" Trp655 and "horizontal" Asp657 that resulted in the photoinactive orange absorbing subpopulation.[33] For the eight proteins, the sequence alignment of every protein had a Trp and Asp residue at the corresponding locations of Trp655 and Asp657 in NpR6012g4, except for NpR1597g4, which had a valine (Val) and all had Asp (Figure S8).[47] This highly conserved sequence suggest that there may be similar lid Trp and horizontal/vertical Asp orientations for all these systems, but NMR or X-ray crystallography would need to be performed to confirm. Assuming that all of these proteins have Asp in this location suggest that the Asp in the proteins that do not exhibit the photoinactive Lumi-O_f either does not have the vertical Asp orientation or the Asp does not interact with the chromophore.

Several CBCRs do not complete the photocycle within the 1 ms probe delay and several CBCRs only require the $^{15Z}P_r$ signals (shaded region) to fit the data. NpR1597g4, NpF2164g4, NpF2854g3, and NpR4776g3 exhibit the sequential evolution of photoproduct species after excitation with no apparent Lumi-O_f photoproduct dynamics. The remaining CBCRs (NpAF142g2, NpF2164g6, NpR4776g2, and NpR6012g4) exhibit multiphasic decay kinetics, which Lumi-O_f spectra exhibiting broad and blue shifted bleach bands near 600 nm. The new photoproduct with blue-shifted features likely evolves from the excitation of the 600-nm P_o subpopulation. Like NpF2164g7 and RcaE, half of the CBCRs presented here have inhomogeneity that persist to the Lumi state, suggesting that inhomogeneity lasting past the initial excited states may be a consistent trend for some CBCRs.[32, 34] Similar ground-state inhomogeneity and

excitation-wavelength-dependences have been reported for CBCRs and related photoreceptor proteins.[14, 48] Keeping consistency with NpR6012g4, all of Lumi-O_f states observed had shorter lifetimes than the Lumi-R_f state and failed to evolve to a Meta state, except for NpAF142g2 which unproductive Lumi-O_f state had a longer lifetime than the productive Lumi-R_f state (Table 1).[33]

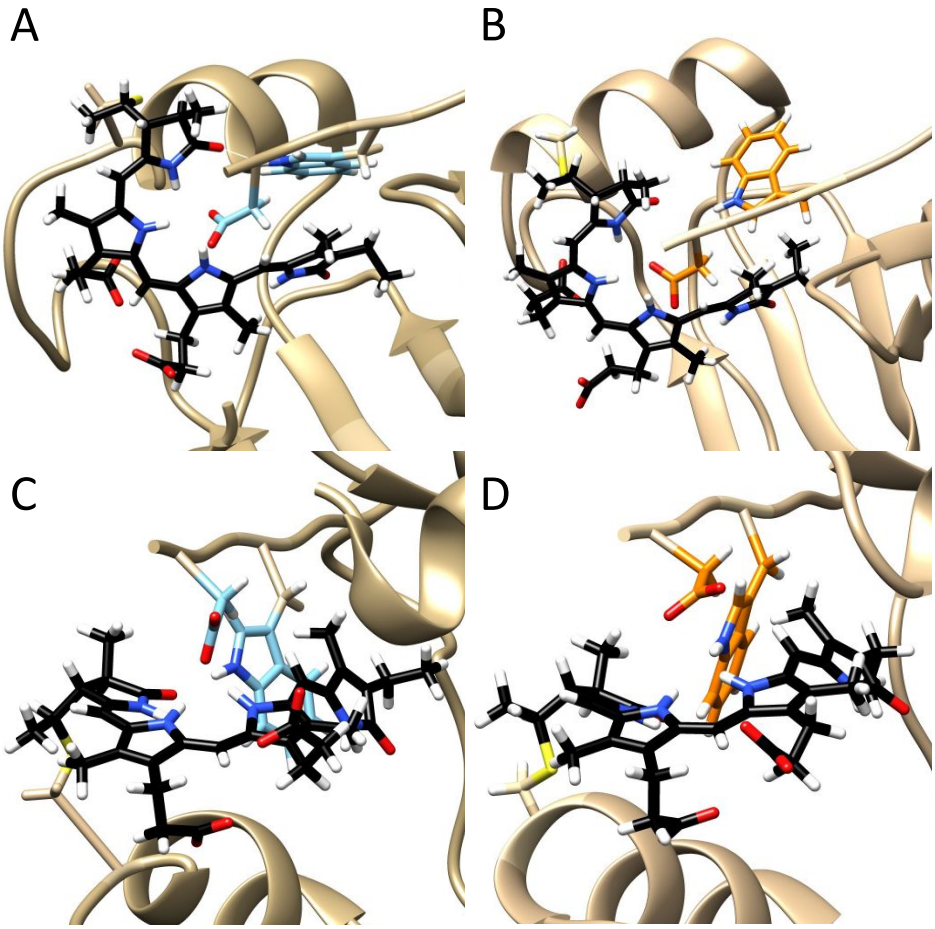

Figure 8. Structural heterogeneity of Trp655 and Asp657 of the $^{15Z}P_r$ state (6BHN) that results in the red absorbing (left column, blue amino acid residues)) and orange absorbing (right column, orange amino acid residues) subpopulations. For the red absorbing subpopulation Trp655 overlaps with the D-ring (A) and H-bonds with the A-ring of the PCB chromophore and Asp657 is in a "vertical" orientation (C) that can also H-bond to the chromophore. In the orange absorbing subpopulation Trp655 is rotated away from the D-ring (B) and the Asp657 is in a "horizontal" configuration (D) that cannot H-bond to the chromophore.

8/27/2019 4:11 AM

NpR1597g4 had a Val in place of Trp, for the Trp/Asp requirements for the $^{15Z}P_o$ subpopulation,[33] but since NpR1597g4 did not exhibit features associated with the $^{15Z}P_o$ subpopulations this does not shed much light on the amino acid residue requirements for the unproductive $^{15Z}P_o$ subpopulation. Interestingly, given the amino acid sequences previously reported by Rockwell et al.[44, 47] (Figures S9 and S10), all of the domains that exhibited features of the unproductive $^{15Z}P_o$ subpopulation incorporate a glycine residue (except for NpR6012g4) at T631 of NpR6012g4 and all the domains that did not exhibit features of the $^{15Z}P_o$ subpopulation incorporate a serine residue at this location. To determine if the serine or glycine amino acid residue at this location is indicative of the presence or lack thereof, of the $^{15Z}P_o$ subpopulation, further studies can probe the secondary dynamics of difference Red/Green CBCRs with reported serine or glycine amino acid residues at this location (Figure S10), such as AnPixJg2, AnPixJg3, AnpixJg4, NpR5113g2, etc.

CONCLUDING COMMENTS

The secondary photodynamics of several red/green photoswitching CBCRs from the cyanobacterial *N. punctiforme* were characterized with transient absorption spectroscopy from ns to ms. It was observed that all nine *N. punctiforme* CBCR samples had a consistent trend of blue shifting intermediates, suggesting that the evolution from Z-to-E is a smooth, sustained transition. Also, all of the samples other than NpR1597g4 and NpF477g3 had a continuous blue shift of each intermediate to a new color region whereas the final evolution for these two proteins remained in the same region (yellow). This consistent blue-shifting with evolution was also observed in NpF2164g7.[32] Similar to the ultrafast studies, the protein samples were classified into categories based on the nature of the photodynamics: CBCRs exhibiting or not exhibiting a Lumi-O_f photoproduct. Considering that half of the CBCRs presented here had heterogeneity past the initial

excited states suggest that heterogeneity persisting to the secondary photoproducts may be more common than originally thought. It is clear that the inhomogeneity present in the ultrafast dynamics carries over to some degree into the secondary timescale.[18] The exact causes of the distinctions between the timescales of all the CBCRs, however, are not known and elucidation of this will require more extensive structural and spectroscopic studies.

ACKNOWLEDGEMENTS

This work was supported by a grant from the Chemical Sciences, Geosciences, and Biosciences Division, Office of Basic Energy Sciences, Office of Science, United States Department of Energy (DOE DE-FG02-09ER16117) to both J.C.L. and D.S.L. Nathan C. Rockwell (University of California, Davis) is acknowledged for sample preparation and constructive discussions. Dr. Mikas Vengris (Light Conversion Ltd.) is also acknowledged for the donation of global and target analysis software.

8/27/2019 4:11 AM

REFERENCES

1. Van der Horst, M. A. and K. J. Hellingwerf Photoreceptor proteins, "star actors of modern times": A review of the functional dynamics in the structure of representative members of six different photoreceptor families. *Acc. Chem. Res.*, 2004, **37,** 13-20.
2. Rockwell, N. C. and J. C. Lagarias A Brief History of Phytochromes. *Chemphyschem*, 2010, **11,** 1172-1180.
3. Möglich, A., X. J. Yang, R. A. Ayers and K. Moffat Structure and Function of Plant Photoreceptors. *Annu. Rev. Plant Biol.*, 2010, **61,** 21-47.
4. Briggs, W. R. and J. L. Spudich (2005) Handbook of Photosensory Receptors. pp. 473. Wiley-VCH, Weinheim, Germany.
5. Rockwell, N. C., Y. S. Su and J. C. Lagarias Phytochrome structure and signaling mechanisms. *Annu. Rev. Plant Biol.*, 2006, **57,** 837-858.
6. Franklin, K. A. and P. H. Quail Phytochrome functions in Arabidopsis development. *J. Exp. Bot.*, 2010, **61,** 11-24.
7. Quail, P. H. Phytochrome photosensory signalling networks. *Nat. Rev. Mol. Cell Biol.*, 2002, **3,** 85-93.
8. De Riso, V., R. Raniello, F. Maumus, A. Rogato, C. Bowler and A. Falciatore Gene silencing in the marine diatom Phaeodactylum tricornutum. *Nucleic Acids Res.*, 2009, **37**.
9. Blumenstein, A., K. Vienken, R. Tasler, J. Purschwitz, D. Veith, N. Frankenberg-Dinkel and R. Fischer The Aspergillus nidulans phytochrome FphA represses sexual development in red light. *Current biology : CB*, 2005, **15,** 1833-1838.
10. Froehlich, A. C., B. Noh, R. D. Vierstra, J. Loros and J. C. Dunlap Genetic and molecular analysis of phytochromes from the filamentous fungus Neurospora crassa. *Eukaryot. Cell*, 2005, **4,** 2140-2152.
11. Rockwell, N. C. and J. C. Lagarias The structure of phytochrome: A picture is worth a thousand spectra. *Plant Cell*, 2006, **18,** 4-14.
12. Narikawa, R., Y. Fukushima, T. Ishizuka, S. Itoh and M. Ikeuchi A novel photoactive GAF domain of cyanobacteriochrome AnPixJ that shows reversible green/red photoconversion. *J. Mol. Biol.*, 2008, **380,** 844-855.
13. Freer, L. H., P. W. Kim, S. C. Corley, N. C. Rockwell, L. Zhao, A. J. Thibert, J. C. Lagarias and D. S. Larsen Chemical Inhomogeneity in the Ultrafast Dynamics of the DXCF Cyanobacteriochrome Tlr0924. *J. Phys. Chem. B*, 2012, **116,** 10571-10581.
14. Kim, P. W., L. H. Freer, N. C. Rockwell, S. S. Martin, J. C. Lagarias and D. S. Larsen Second-Chance Forward Isomerization Dynamics of the Red/Green Cyanobacteriochrome NpR6012g4 from Nostoc punctiforme. *J. Am. Chem. Soc.*, 2012, **134,** 130-133.
15. Chang, C. W., S. M. Gottlieb, P. W. Kim, N. C. Rockwell, J. C. Lagarias and D. S. Larsen Reactive Ground-State Pathways Are Not Ubiquitous in Red/Green Cyanobacteriochromes. *Journal of Physical Chemistry B*, 2013, **117,** 11229-11238.
16. Gottlieb, S. M., P. W. Kim, S. C. Corley, D. Madsen, S. J. Hanke, C. W. Chang, N. C. Rockwell, S. S. Martin, J. C. Lagarias and D. S. Larsen Primary and secondary photodynamics of the violet/orange dual-cysteine NpF2164g3 cyanobacteriochrome domain from Nostoc punctiforme. *Biochemistry*, 2014, **53,** 1029-1040.
17. Gottlieb, S. M., C. W. Chang, S. S. Martin, N. C. Rockwell, J. C. Lagarias and D. S. Larsen Optically Guided Photoactivity: Coordinating Tautomerization, Photoisomerization, Inhomogeneity, and Reactive Intermediates within the RcaE Cyanobacteriochrome. *J Phys Chem Lett*, 2014, **5,** 1527-1533.
18. Gottlieb, S. M., P. W. Kim, C.-W. Chang, S. J. Hanke, R. J. Hayer, N. C. Rockwell, S. S. Martin, J. C. Lagarias and D. S. Larsen Conservation and Diversity in the Primary Forward Photodynamics of Red/Green Cyanobacteriochromes. *Biochemistry*, 2015, **54,** 1028-1042.

19. Narikawa, R., T. Ishizuka, N. Muraki, T. Shiba, G. Kurisu and M. Ikeuchi Structures of cyanobacteriochromes from phototaxis regulators AnPixJ and TePixJ reveal general and specific photoconversion mechanism. *Proc. Natl. Acad. Sci.*, 2013, **110,** 918-923.
20. Yoshihara, S. and M. Ikeuchi Phototactic motility in the unicellular cyanobacterium Synechocystis sp. PCC 6803. *Photochem. Photobiol. Sci.*, 2004, **3,** 512-518.
21. Hirose, Y., T. Shimada, R. Narikawa, M. Katayama and M. Ikeuchi Cyanobacteriochrome CcaS is the green light receptor that induces the expression of phycobilisome linker protein. *Proc. Natl. Acad. Sci.*, 2008, **105,** 9528-9533.
22. Kehoe, D. M. and A. Gutu Responding to color: The regulation of complementary chromatic adaptation. *Annu. Rev. Plant Biol.*, 2006, **57,** 127-150.
23. Campbell, E. L., K. D. Hagen, R. Chen, D. D. Risser, D. P. Ferreira and J. C. Meeks Genetic Analysis Reveals the Identity of the Photoreceptor for Phototaxis in Hormogonium Filaments of <span class="named-content genus-species" id="named-content-1">Nostoc punctiforme</span&gt. *Journal of Bacteriology*, 2015, **197,** 782.
24. Kim, P. W., L. H. Freer, N. C. Rockwell, S. S. Martin, J. C. Lagarias and D. S. Larsen Femtosecond Photodynamics of the Red/Green Cyanobacteriochrome NpR6012g4 from Nostoc punctiforme. 1. Forward Dynamics. *Biochemistry*, 2012, **51,** 608-618.
25. Kim, P. W., L. H. Freer, N. C. Rockwell, S. S. Martin, J. C. Lagarias and D. S. Larsen Femtosecond Photodynamics of the Red/Green Cyanobacteriochrome NpR6012g4 from Nostoc punctiforme. 2. Reverse Dynamics. *Biochemistry*, 2012, **51,** 619-630.
26. Kim, P. W., L. H. Freer, N. C. Rockwell, S. S. Martin, J. C. Lagarias and D. S. Larsen Second-Chance Forward Isomerization Dynamics of the Red/Green Cyanobacteriochrome NpR6012g4 from Nostoc punctiforme. *Journal of the American Chemical Society*, 2012, **134,** 130-133.
27. Slavov, C., X. Xu, K.-h. Zhao, W. Gärtner and J. Wachtveitl Detailed insight into the ultrafast photoconversion of the cyanobacteriochrome Slr1393 from Synechocystis sp. *Biochimica et Biophysica Acta (BBA) - Bioenergetics*, 2015, **1847,** 1335-1344.
28. Pennacchietti, F., A. Losi, X. L. Xu, K. H. Zhao, W. Gartner, C. Viappiani, F. Cella, A. Diaspro and S. Abbruzzetti Photochromic conversion in a red/green cyanobacteriochrome from Synechocystis PCC6803: quantum yields in solution and photoswitching dynamics in living E. coli cells. *Photochem Photobiol Sci*, 2015, **14,** 229-237.
29. Fukushima, Y., M. Iwaki, R. Narikawa, M. Ikeuchi, Y. Tomita and S. Itoh Photoconversion Mechanism of a Green/Red Photosensory Cyanobacteriochrome AnPixJ: Time-Resolved Optical Spectroscopy and FTIR Analysis of the AnPixJ-GAF2 Domain. *Biochemistry*, 2011, **50,** 6328–6339.
30. Narikawa, R., Y. Fukushima, T. Ishizuka, S. Itoh and M. Ikeuchi A novel photoactive GAF domain of cyanobacteriochrome AnPixJ that shows reversible green/red photoconversion. *Journal of Molecular Biology*, 2008, **380,** 844-855.
31. Xu, X. L., A. Gutt, J. Mechelke, S. Raffelberg, K. Tang, D. Miao, L. Valle, C. D. Borsarelli, K. H. Zhao and W. Gartner Combined mutagenesis and kinetics characterization of the bilin-binding GAF domain of the protein Slr1393 from the Cyanobacterium Synechocystis PCC6803. *Chembiochem*, 2014, **15,** 1190-1199.
32. Kirpich, J. S., C.-W. Chang, D. Madsen, S. M. Gottlieb, S. S. Martin, N. C. Rockwell, J. C. Lagarias and D. S. Larsen Noncanonical Photodynamics of the Orange/Green Cyanobacteriochrome Power Sensor NpF2164g7 from the PtxD Phototaxis Regulator of Nostoc punctiforme. *Biochemistry*, 2018, **57,** 2636-2648.
33. Sunghyuk Lim, Q. Y., Sean M. Gottlieb, Che-Wei Chang, Nathan C. Rockwell, Shelley S. Martin, Dorte Madsen, J. Clark Lagarias, Delmar S. Larsen, and James B. Ames Correlating structural and photochemical heterogeneity in cyanobacteriochrome NpR6012g4. *Proc. Nati. Acad. Sci. USA*, 2018, **115,** 4387-4392.

8/27/2019 4:11 AM

34. Chang, C.-W., S. M. Gottlieb, N. C. Rockwell, S. S. Martin, J. C. Lagarias and D. S. Larsen Tracking the secondary photodynamics of the green/red cyanobacteriochrome RcaE from Fremyella diplosiphon. *Chem. Phys. Lett.*, 2016, **644,** 225-230.
35. Kirpich, J. S., S. M. Gottlieb, C.-W. Chang, P. W. Kim, S. S. Martin, J. C. Lagarias and D. S. Larsen Forward Photodynamics of the Noncanonical Red/Green NpR3784 Cyanobacteriochrome from Nostoc punctiforme. *Biochemistry*, 2019, **58,** 2297-2306.
36. Xu, X. L., A. Gutt, J. Mechelke, S. Raffelberg, K. Tang, D. Miao, L. Valle, C. D. Borsarelli, K. H. Zhao and W. Gärtner Combined Mutagenesis and Kinetics Characterization of the Bilin-Binding GAF Domain of the Protein Slr1393 from the Cyanobacterium Synechocystis PCC6803. *ChemBioChem*, 2014, **15,** 1190-1199.
37. Edgar, R. C. MUSCLE: multiple sequence alignment with high accuracy and high throughput. *Nucleic Acids Res.*, 2004, **32,** 1792-1797.
38. Rockwell, N. C., L. Shang, S. S. Martin and J. C. Lagarias Distinct classes of red/far-red photochemistry within the phytochrome superfamily. *Proc. Natl. Acad. Sci. U S A*, 2009, **106,** 6123-6127.
39. Gambetta, G. A. and J. C. Lagarias Genetic engineering of phytochrome biosynthesis in bacteria. *Proc. Nati. Acad. Sci. USA*, 2001, **98,** 10566-10571.
40. Carroll, E. C., O. C. Compton, D. Madsen, F. E. Osterloh and D. S. Larsen Ultrafast carrier dynamics in exfoliated and functionalized calcium niobate nanosheets in water and methanol. *J. Phys. Chem. C*, 2008, **112,** 2394-2403.
41. Spillane, K. M., J. Dasgupta, J. C. Lagarias and R. A. Mathies Homogeneity of Phytochrome Cph1 Vibronic Absorption Revealed by Resonance Raman Intensity Analysis. *J. Am. Chem. Soc.*, 2009, **131,** 13946-13948.
42. van Stokkum, I. H. M., D. S. Larsen and R. van Grondelle Global and target analysis of time-resolved spectra. *Biochim. Biophys. Acta*, 2004, **1657,** 82-104.
43. Holzwarth, A. R. (1996) Data Analysis of Time-Resolved Measurements. In *Biophysical techniques in photosynthesis*. (Edited by J. Amesz and A. J. Hoff), pp. 75-92. Springer, Netherlands.
44. Rockwell, N. C., S. S. Martin, A. G. Gulevich and J. C. Lagarias Conserved phenylalanine residues are required for blue-shifting of cyanobacteriochrome photoproducts. *Biochemistry*, 2014, **53,** 3118-3130.
45. Velazquez Escobar, F., T. Utesch, R. Narikawa, M. Ikeuchi, M. A. Mroginski, W. Gartner and P. Hildebrandt Photoconversion mechanism of the second GAF domain of cyanobacteriochrome AnPixJ and the cofactor structure of its green-absorbing state. *Biochemistry*, 2013, **52,** 4871-4880.
46. Rockwell, N. C., S. S. Martin, K. Feoktistova and J. C. Lagarias Diverse two-cysteine photocycles in phytochromes and cyanobacteriochromes. *Proc Natl Acad Sci U S A*, 2011, **108,** 11854-11859.
47. Rockwell, N. C., S. S. Martin and J. C. Lagarias Red/Green Cyanobacteriochromes: Sensors of Color and Power. *Biochemistry*, 2012, **51,** 9667-9677.
48. Gottlieb, S. M., P. W. Kim, N. C. Rockwell, Y. Hirose, M. Ikeuchi, J. C. Lagarias and D. S. Larsen Primary photodynamics of the green/red-absorbing photoswitching regulator of the chromatic adaptation E domain from Fremyella diplosiphon. *Biochemistry*, 2013, **52,** 8198-8208.